Carbon-based hybrid materials: growth, characterization and investigation of properties

Arshad, Muhammad

Chapter 4

Aligned and unaligned carbon nanotubes: growth and photoinduced charge transfer mechanism*

This chapter is dedicated to the controlled synthesis of carbon nanotubes (CNTs) and the photoinduced charge transfer behaviour of aligned and unaligned CNTs. Time-resolved reflectivity measurements performed on these CNTs with a pump energy quasi-resonant with the second Van Hove singularity of semiconducting tubes revealed a positive sign of the transient reflectivity in unaligned nanotubes, whereas a negative sign was detected in aligned nanotubes. This discovery addresses a long-standing question showing that in unaligned nanotubes the stronger intertube interactions favour the formation of short-lived free charge carriers in semiconducting tubes. A detailed analysis of the transient reflectivity spectral response shows that the free carriers in the photoexcited state of semiconducting tubes move towards metallic tubes in about 400 fs.

*__The results presented in this chapter were published in:__ G. Galimberti, S. Pagliara, S. Ponzoni, S. Dal Conte, F. Cilento, G. Ferrini, S. Hofmann, M. Arshad, C. Cepek and F. Parmigiani, “The photoinduced charge transfer mechanism in aligned and unaligned carbon nanotubes”, *Carbon*, *49*(15), 5246-5252 (2011).

4.1 Introduction

The electronic and electrical transport properties of single-walled carbon nanotubes (SWCNTs) are strongly affected by structure and by their organization in form of bundles, their orientation, chirality and intertube interactions. Bundled CNTs inherently comprise of mixture of metallic and semiconductor tubes. During the last years a significant effort has been dedicated to the synthesis of CNTs with controlled orientation and their realization into electronic devices. The efficiency of CNT-based devices, ranging from field effect transistors to nano-photovoltaic systems, strongly depends on non-equilibrium carrier transport and on charge transfer mechanisms from semiconducting to metallic nanotubes. [1-4] Therefore, an accurate understanding of the interactions between nanotubes and of the charge transfer mechanisms is crucial for a significant advancement of the technology of CNT-based devices.

A large number of studies have revealed that at equilibrium [5-7] the intertube interactions in SWCNT bundles are weak and very analogous to the coupling between adjacent graphene planes in 3D crystalline graphite or the interball coupling found in solid C_{60}. This weak intertube interaction is controlled by the van der Waals forces with a nonzero covalent bond contribution. This behaviour has a substantial impact on the vibrational [5 6 8-11] and electronic properties of nanotubes [12-14] such as band gap openings and pseudogaps in SWCNTs, single electron transport and resistivity. However, the effect of the intertube interactions in bundled SWCNTs, pertinent to charge transfer mechanisms, remains unclear.

A number of theoretical studies have discussed the interactions between adjacent tubes in bundled nanotubes. These studies suggest that the dominant intertube van der Waals interactions, while promoting the nanotube bundling, have the effect of energy shifting and broadening the optical transitions. In particular, the broadening of the absorption spectral features in bundled nanotubes originates from the intertube electronic properties perpendicular to the tube axis. Moreover, the curvature of the nanotube wall in CNTs induces a downshift of the conduction bands by

enhancing the σ–π hybridization. [6 15 16]

Although these mechanisms are well understood, the absence of a strong luminescence in CNT bundles remains unclear. This is a key question concerning the charge transfer processes since it has been argued that the non-radiative channel, quenching the radiative channel (fluorescence), can originate from possible charge transfer from the semiconducting to the metallic tubes. Nevertheless, this is still an open question and optical spectroscopies in the time domain, with a suitable time resolution, might reveal the changes of the optical properties induced by nonradiative mechanisms. [17-20] Recently, this kind of experiments has been performed on CNTs with a well-defined chirality. However, making CNTs with a defined structure and with intertube interactions not affected from other atomic species (contaminants, surfactants or molecule) still remains a major challenge.[21 22] In this framework, in order to highlight the dependence of the charge transfer channel on the bare intertube interactions, time-resolved reflectivity measurements on the femtosecond timescale were carried out on aligned and unaligned SWCNT bundles with different chirality, synthesized by chemical vapour deposition (CVD).[23]

The experiments were performed by using a conventional one-colour pump–probe set-up (pump and probe both at 1.55 eV), along with a novel pump-probe set-up in which the probe is a broadband white light pulse (supercontinuum). [24] By using the supercontinuum pulse as a probe, it is possible to achieve spectral resolution: this allows detecting in the frequency domain the relaxation dynamics of carriers excited through a resonant absorption transition into the conduction band. By setting the pump frequency quasi-resonant with the second Van Hove singularity of the carbon compounds a positive sign of the transient reflectivity was detected in unaligned nanotubes, whereas a negative transient reflectivity was detected in aligned nanotubes. This important difference demonstrates that in unaligned nanotubes the stronger intertube interactions favour the formation of short-living free charge carriers in semiconducting tubes that decay through a charge transfer nonradiative process toward the metallic tubes. A detailed analysis of the transient reflectivity spectral response

shows that the free carriers in the photo-excited state of semiconducting tube transfer to the metallic tubes in about 400 fs.

4.2 Growth of carbon nanotubes

Unaligned and aligned CNT bundles (see scanning electron microscopy (SEM) images in figures 4.1 and 4.2, respectively) were synthesized by CVD on *Si/SiO_2/Al_2O_3 and Si/TiN* substrates in the Analytical Division of the TASC-IOM-CNR laboratory. The catalyst depositions and CVD processes were performed in an ultra-high vacuum experimental apparatus (base pressure<$1x10^{-10}$ mbar). In this apparatus it is possible to control the chemical state of the catalyst (before and after the growth) via X-ray photoelectron spectroscopy (XPS) and to monitor precisely all the CVD parameters (*i.e*. precursor gas purity, pressure and pressure gradient, sample temperature, gas fluxes, *etc*.).

The CVD was performed on 150 nm thick films of SiO_2 thermally grown on polished n-type Si (100) substrates [25]; on 10 nm thick Al_2O_3 films grown via magnetron sputtering [26] on the previous film and on 30 nm TiN films grown via atomic layer deposition (ALD) on Si substrates. [27] We used Fe as catalyst, and acetylene as the precursor gas. The Fe catalyst thin films were deposited *in situ* at a growth rate of ~0.6 nm/h on substrates at room temperature by sublimation from filaments (Aldrich, 99.9% purity) heated by electron bombardment. The deposition rate was determined from the attenuation of the photoemission peaks of Al 2*p* for the Al_2O_3 support layer and Si 2*p* for the SiO_2 support layer.

The samples were clamped between two tantalum contacts for direct heating. The Fe films were always monitored by X-ray photoelectron spectroscopy (XPS) to detect the presence of contaminants. We operated in the following parameters window: ≈0.6–8 nm Fe film thickness, 4×10^{-8}–10^{-3} mbar C_2H_2 pressure (≈ 4 sccm) and 580–600°C growth temperature. A typical CVD route consisted of a preliminary out-gassing of the substrate at 550–600 °C, followed by Fe deposition at room temperature, and successive ramping-up to the chosen growth temperature. In order to exclude extrinsic

effects, residual solvents or chemical treatments during the CNTs synthesis were avoided. Figure 4.1 shows the SEM micrograph obtained from growth on Si/TiN in these conditions. The SEM images show a high density of spaghetti-like CNT structures which uniformly covers the substrate. The average diameter of these CNTs is around 1.0 nm (confirmed by Raman) and their length ranges up to several micrometers. When the C_2H_2 flux during the CVD process is significantly increased to 50 sccm, while all the other experimental conditions mentioned above are kept the same, CNTs with the morphology seen in the SEM images in Figure 4.2 are produced; the SEM image shown in the lower panel was taken at the edge of the nanotube-covered area. These SEM images show a forest-like dense

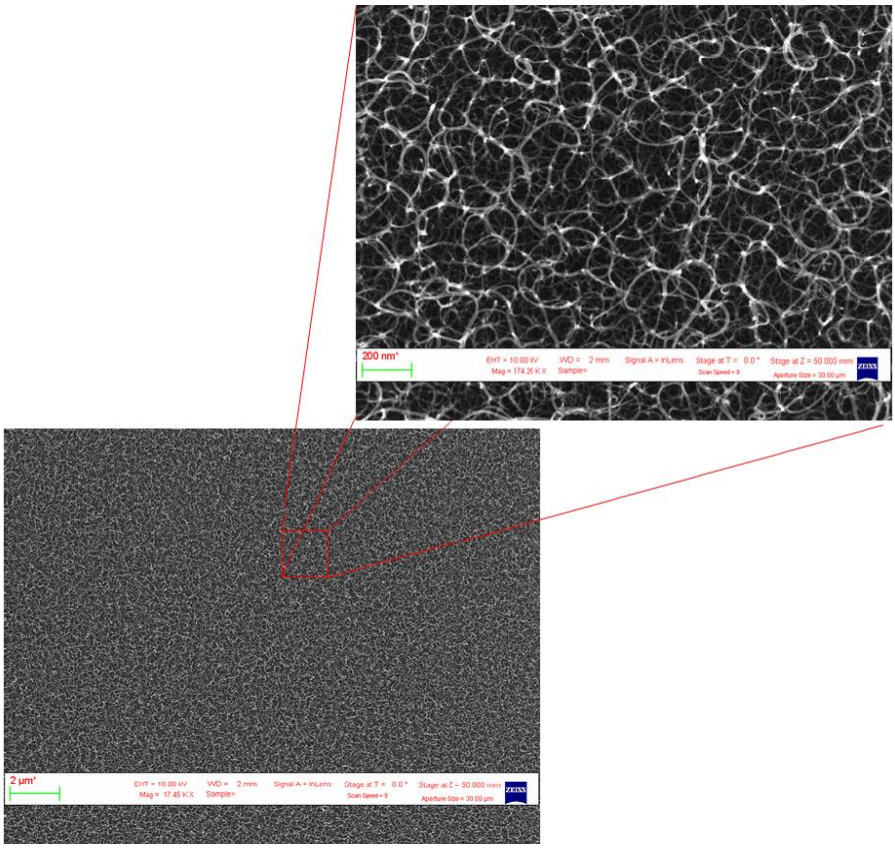

Figure 4.1: SEM images of unaligned SWCNTs grown on Si/TiN substrate

growth of vertically aligned self-supported CNTs. The average diameter of these CNTs ranges from 1 to 1.6 nm (confirmed by Raman) and their length is around 4 to 5 µm.

The TiN and Al_2O_3 buffer layers are deposited on top of the SiO_2/Si substrates to prevent the diffusion of catalyst into Si and to avoid the formation of metal silicide during pretreatments and during CNT growth.[28] The introduction of a buffer layer between catalyst and SiO_2/Si substrate also facilitates the CNT growth and in particular a Al_2O_3 layer is used for the growth of dense and aligned SWCTs because it increases the roughness of the surface and thereby creates more nucleation sites.[29 30]

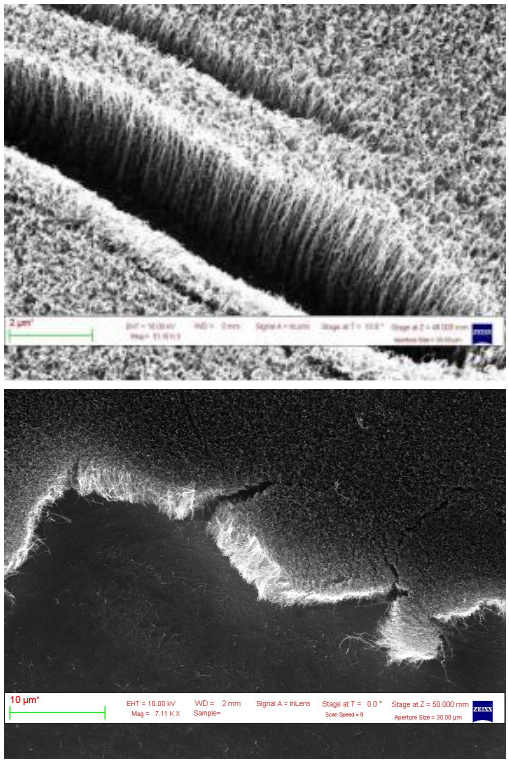

Figure 4.2: SEM images of vertically aligned SWCNT carpets grown on Al_2O_3/SiO_2/Si substrates

4.3 Results and discussion

4.3.1 Raman analysis

The micro-Raman measurements were carried out on the dense aligned and on the unaligned SWCNTs. As shown in figure 4.3, the presence of radial breathing modes (RBMs) in aligned and unaligned CNT carpets characterize them as SWCNTs. For aligned CNTs, the main RBM peak is located around 165 cm^{-1} along with one larger structure corresponding to a diameter range from 1 to 1.6 nm. [31] For the unaligned CNTs, the D and G bands and the signal from the Si substrate are marked (see figure 4.3 (b)). The D band is usually assigned to defects, whereas the G band is more structured, which indicates a better quality of the SWCNTs. The RBMs for the unaligned CNTs are at 225 cm^{-1} and 300 cm^{-1}. By using the relation $\omega_{rgb} = B + (A/d^n)$, with A = 234 cm^{-1} and B = 10 cm^{-1}, the estimated diameters of the nanotubes [31] range between

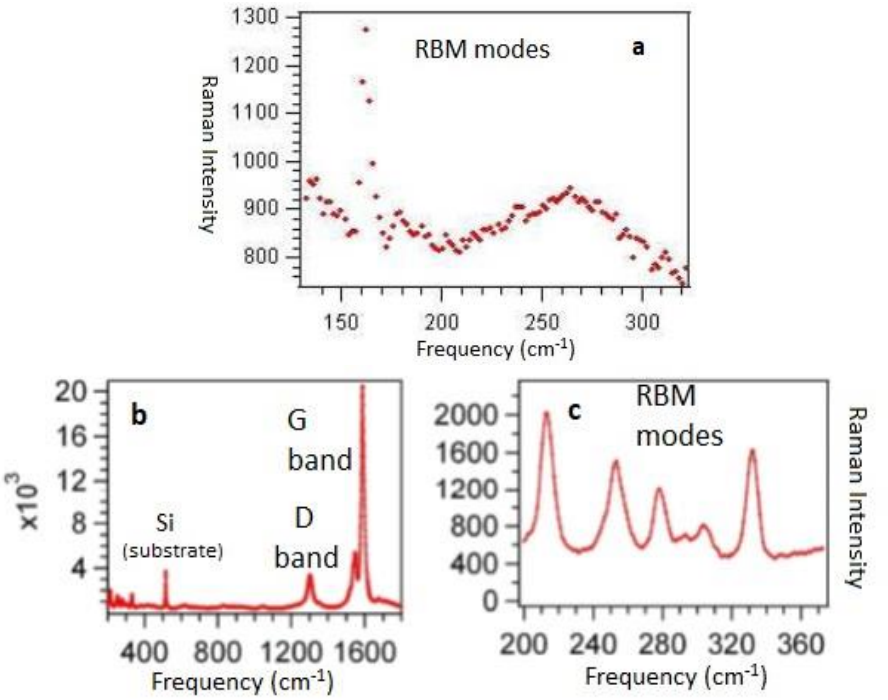

Figure 4.3: Micro-Raman spectrum collected from aligned (a) and unaligned (b, c) SWCNTs with a He-Ne laser source (λ=632.8 nm).

0.8 nm and 1.2 nm. The average diameter is about 1.0 nm.

4.3.2 Transient reflectivity measurements

The evaluation of the diameters from Raman spectroscopy is consistent with the results of the static reflectivity measurement. In fact, it is possible to evaluate the nanotube diameter from the energy positions of the features in the static reflectivity spectrum, ascribed to interband optical transitions from various valence subbbands to their respective conduction subbands. Because of the one-dimensional nature of the electronic bands, the density of states of SWCNTs exhibits a series of characteristic Van Hove singularities (VHSs) detectable in the near IR and visible spectral regions. By using the Kataura scheme [32] in order to compare in particular the second Van Hove singularity transitions in the two cases, we obtained the scheme shown in figure 4.4. It is evident that in both cases, with a pump and probe

energies of 1.5 eV, we should expect a photobleaching effect and it is what we get in the case of aligned CNT, but not on the unaligned CNT sample.

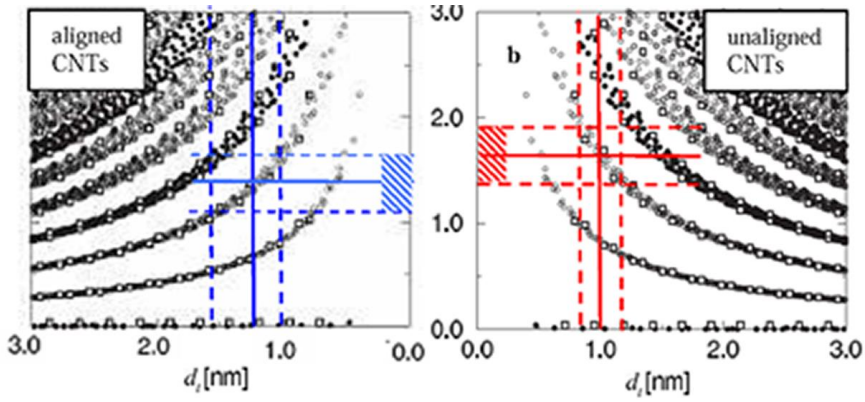

Figure 4.4: Static reflectivity spectrum collected from aligned and unaligned carbon nanotube samples.

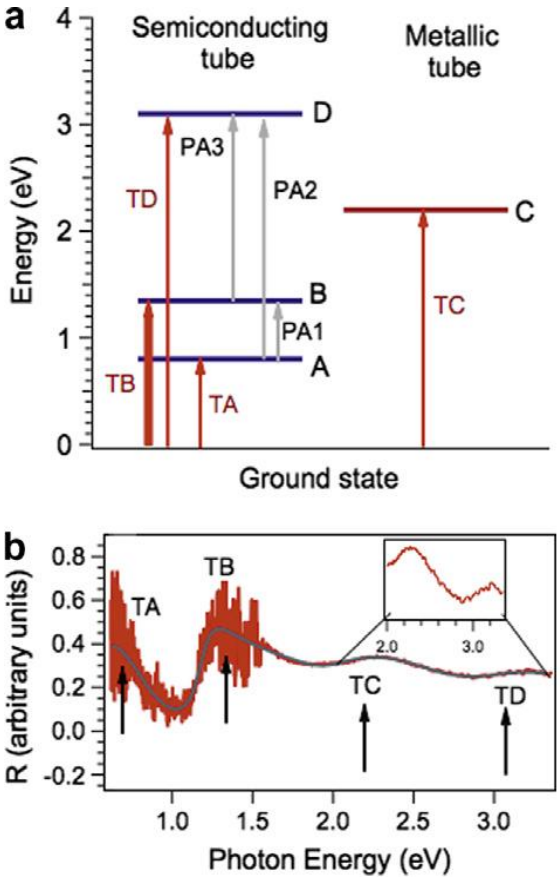

Figure 4.5: (a) Schematic electronic structure of both semiconducting and metallic unaligned bundled SWNTs. The energy positions of the bands (A, B, C and D) are estimated by the reflectivity spectrum reported in (b). The arrows TA, TB, TC and TD indicate the transitions from the ground state to unoccupied states. PA1, PA2 and PA3 refer to photoabsorption processes induced by the laser pump nearly resonant with the TB transition.

Figure 4.5 (a) presents the schematic electronic structure of both semiconducting and metallic unaligned bundled SWNTs which gives rise to the reflectivity spectrum, collected on unaligned SWNT bundles, shown in Figure 4.5 b. Four structures located at about 0.8 eV (TA), 1.35 eV (TB), 2.2 eV (TC) and 3.1 eV (TD) are clearly detected. TA, TB and TD are assigned to the inhomogeneously broadened interband optical transitions from the valence subbands to their respective conduction subbands in semiconducting SWCNTs as schematically shown in figure 4.5 (a). Instead, the band TC is assigned to an interband transition in metallic SWCNTs. [17 18]

When the photon pump energy is resonant with a VHS, a transient photobleaching is usually expected in the one-colour time-resolved optical spectroscopy. Absorption of the pump pulse excites electrons into the conduction band, creating holes in the valence band. Until these carriers relax, transient filling effects on the final states are observed. For the photobleaching effect, the transient signal is positive in trasmittivity and negative in reflectivity (as in absorption). [18-20 33]

Figure 4.6 shows the one-colour transient reflectivity on unaligned SWCNT bundles (see SEM image figure 4.1) together with the spectrum acquired on aligned SWCNT bundles (see SEM image figure 4.2). The negative transient reflectivity signal on the aligned SWCNTs reveals the photobleaching process in agreement with literature [18-20 34], the positive transient reflectivity signal on unaligned SWCNTs is the fingerprint of a new

relaxation channel that increases the reflectivity. For the assignment of the spectral features we refer to the scheme in Figure 4.6 (a). We attribute the positive transient reflectivity signal to a free-electron like character of the carriers excited in the B band of semiconducting tubes. The transient reflectivity's negative sign of the substrate including the catalyst nanoparticles suggests that the contribution of the substrate (inset in figure 4.6 (b)) is negligible. Moreover, the different orientation of the laser polarization with respect to the nanotube axis in the unaligned and aligned bundles cannot justify a different sign in the transient optical response.

At this pump photon energy, the VHS optical transitions are excited only with an electric field parallel to the nanotube axis. Due to the near-normal incidence of the laser pump, we expect strong excitation mainly in the unaligned bundles, where the laser polarization, in a statistical sense, can be found parallel to the tube axis. [35] However, also in the vertically aligned bundles the excitation of the VHS transitions cannot be excluded even at near normal incidence, considering the imperfect alignment of the CNTs that

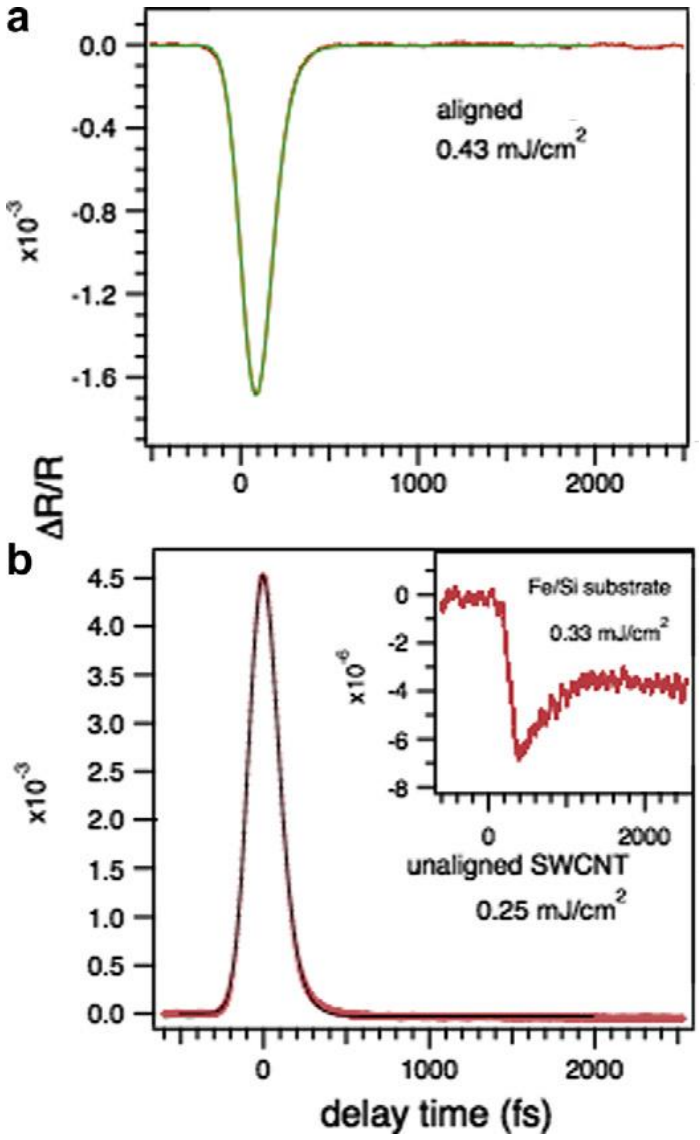

Figure 4.6: One colour (hv = 1.55 eV, fluence of 0.2 mJ/cm^2) transient reflectivity spectra collected on both aligned (a) and unaligned (b) SWCNT. The TR spectrum of the substrate is also reported (inset in (b)) in order to exclude its contribution on the TR signal of unaligned bundles. The spectra of unaligned and aligned SWCNTs are well fitted with one exponential curve convoluted with a Gaussian (representing the laser pulsewidth).

prevents them from being oriented perfectly normal to the incident electric field of the pump beam. As a consequence, the laser pump excites the same VHS transition in both the samples, the only difference being the excitation intensity. In agreement with literature [36 37], due to the dependence of absorption coefficient on the relative CNT – electric field orientation, we conclude that only the density of the photoexcited carriers and not the sign of the transient reflectivity is affected by the excitation of the VHS transitions.

The positive transient reflectivity sign can be rationalized considering that in the aligned SWCNTs the intertube interactions is comparable with the van der Waals interactions among the graphene layers in graphite, whereas in unaligned SWCNT the intertube interactions are changed by both the curvature and the spatial anisotropy. In particular, the modified intertube interactions induce an overlap between the π-bands of adjacent tubes by allowing the delocalization of the electrons photoexcited in the VHS. Usually, the presence of VHSs or of strongly bound excitons inhibits the free-carrier mobility yielding to a localization of charge carriers on a length scale of 100 nm. [38] The modified intertube interactions in the unaligned bundles, on the contrary, delocalize the carriers excited in these bands, inhibiting the photobleaching and favouring the free-electron mobility.
The delocalized charge created as optical response is expected to behave as a Drude electron gas. In this case the imaginary part of the dielectric function can be written as [39]:

$$\varepsilon_2(\omega) = \frac{\omega_p^2 \tau}{\omega(1+\omega^2\tau^2)} \qquad (5.1)$$

where $\omega p = \sqrt{(Ne^2)/\varepsilon_0 m}$ is the plasma frequency, N the carrier density, e and m the charge and the mass of the electron, ε_0 the vacuum dielectric constant.

For an ideal free-electron metal, the reflectivity approaches unity below the plasma frequency. Above the plasma frequency, the metal is transparent and the reflectivity decreases rapidly with increasing frequency. When free-electron carriers are created by the laser pump, the Drude-like behaviour of

the carriers enhances the reflectivity. Therefore, the transient reflectivity, which is the reflectivity signal of the probe modified by the presence of the laser pump, is positive and it can be directly related to the CNTs orientation (aligned or unaligned SWCNTs bundles).

To further support this finding, transient reflectivity measurements on films with different CNTs density, length and substrates have been performed. The transient reflectivity positive signal shows no dependence on these sample characteristics. Moreover, to rule out spurious effects such as nonlinear processes and sample damage the experiments have been repeated varying the laser fluence from 10-80 mJ/cm^2 and from 0.1-0.8 mJ/cm^2 (shown in figure 4.7 (a) and (b)). In figure 4.6 (c) and (d) the dependence of the maximum of the transient reflectivity signal on the pump laser fluence is shown. For the pump fluence ranging from 0.1-0.8 mJ/cm^2 (figure 4.6 (d)), transient reflectivity signal increases with fluence, whereas the saturation effect takes place (figure 4.7 (c)) above 40 mJ/cm^2. To estimate the carrier density excited N(E) in the π^* band the following formula can be used [40]:

$$\int_0^{\infty} N(E)dE = \frac{(1-R)F\alpha}{h\upsilon} \qquad (5.2)$$

where hν is 1.5 eV, the reflectivity R=0.4 and the absorption coefficient $\alpha=2x10^5$ cm^{-1}. Therefore, at laser fluence F=40 mJ/cm^2, the initial photo-

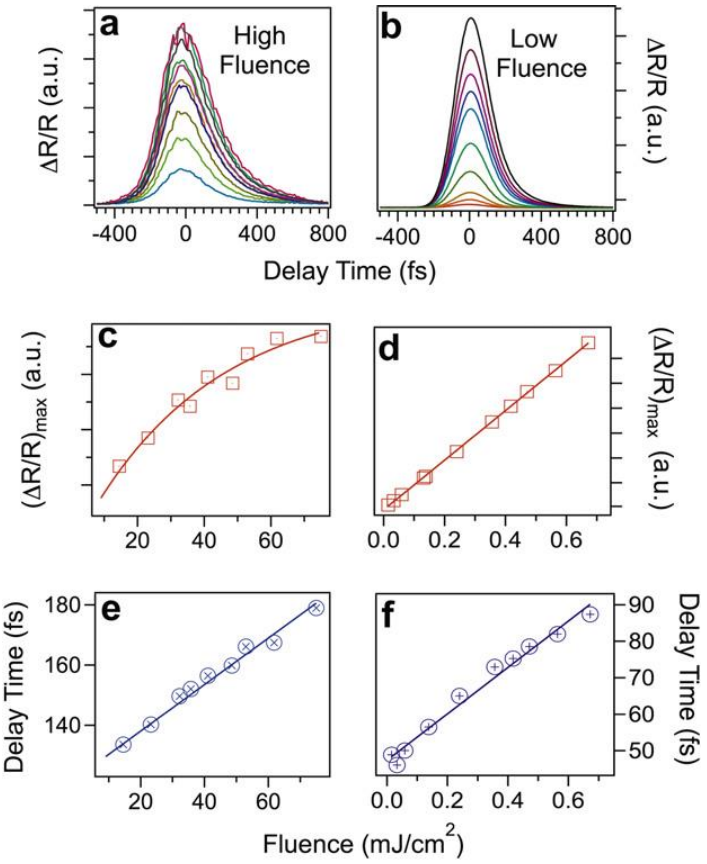

Figure 4.7: (a & b) One-color transient reflectivity spectra collected on unaligned SWCNT bundles by changing the pump laser fluence. The spectra are collected at different fluence regimes: high fluence (from 10 to 80 mJ/cm^2) and low fluence (from 0.1 to 0.8 mJ/cm^2). (c and d) Pump fluence dependence of the maximum of the transient reflectivity spectra and (e and f) of the relaxation time, estimated by fitting the spectra with one exponential decay curve convoluted with a gaussian. The solid curves represent the best fit of these data with a linear (d, e and f) and an exponential curve (c)

carrier density is 20x10^{21} cm^{-3}. This value is comparable (including non-linear optical processes that become important at this high pump fluence) with the carriers density from 0 to 1 eV (6.5x10^{21} cm^{-3}) observed in graphite. [32] This result proves that at the pump intensity used in this experiment and at a photon frequency quasi-resonant with the second VHS, a very high

density of carriers can be excited in the π* band of the semiconducting tube.

To obtain information about the dynamics of the excited- state carriers, the spectra reported in figure 4.3 (a) and (b) are fitted with exponential curves convoluted with a Gaussian representing the laser pulse width. The transient reflectivity spectra of both aligned and unaligned SWCNT bundles are well fitted by one exponential curve with a decay time $(100\mathrm{fs})$ comparable with the laser pulse width (figure 4.6 a and b). Moreover, the dependence of the relaxation time on the fluence (figure 4.7 e and f) excludes radiative recombination processes. [41]

This result is in agreement with the dynamics of the bundles reported in literature [19 37] and it can be justified considering that in CNTs the carrier dynamics strongly depend on the excited state. In particular, when electrons are excited in the first VHS of the semiconducting tubes (A) the lifetime is 1 ps,[19] whereas in the second (B) the lifetime is 130 fs. Meanwhile, the luminescence from isolated CNTs has a longer lifetime (30 ps) than that on unaligned bundles. This can be explained considering that the carriers excited into the second VHS relax very rapidly to the band gap of the semiconducting tube (intraband scattering). Then in isolated nanotubes the electron and the hole recombine across the band gap, whereas, in bundled nanotubes the tunnelling into nearby metallic tubes or into semiconducting tubes with a smaller band gap turns off the luminescence. The excited carriers in the metallic tubes, as shown in time-resolved photoemission experiments, [17 42 43] lose their energy rapidly, therefore quenching the luminescence of CNTs bundles efficiently. [15 17 42 43]

In this experiment, the presence of a fast relaxation channel on unaligned SWCNT bundles confirms that electrons are excited in the second VHS. This behaviour is compatible with a free character of the excited carriers in the semiconducting tubes that favour the charge transfer towards metallic tubes and semiconducting tubes with smaller energy gap. The mechanisms so far described can be understood in more details looking at the optical response of photoexcited SWNTs in both the time and frequency domains.

In these experiments the pump photon energy is 1.55 eV, whereas the probe covers an energy range from 1.1 eV to 2 eV (figure 4.7 (a)). In SWCNTs, a photobleaching process is usually correlated with different photoabsorption channels. [18] In particular, carriers excited in the B band rapidly decay on a giving rise to PA1, PA2 and PA3 photoabsorption processes, where carriers are photoexcited from A to B (PA1), from A to D (PA2) and from B to D (PA3) (see figure 4.5 (a)). By considering the reflectivity spectrum collected on bundled SWCNT sample (figure 4.5 (b)), the photoabsorption channels could appear at 0.60 eV (PA1), 2.3 eV (PA2) and 1.7 eV (PA3).

The 3-dimensional (3D) transient reflectivity spectrum is shown in figure 4.8 (a) together with different extracted line profiles at fixed delay times (figure 4.8 (b) and (c)) or photon energies (figure 4.8 (d) and (e)). The broad red line at about $h\nu$ = 1.55 eV (figure 4.7 (a)) covers the laser pump scattered by the sample. The image profile at delay time τ = 0 fs (figure 4.8 (b)) shows two positive features. The first, broadband and centred at 1.4 eV, is the TB transition; its positive signal confirms the free electron character of the excited carriers discussed in one colour transient reflectivity at 1.55 eV. This band appears structured due to the noise in the measurement. The second positive feature at 1.65 eV is ascribed to the PA3 photoabsorption process. Electrons are excited by the probe from the B band to the D band in the pulsewidth. This picture is confirmed by the lack of relaxation processes before the photoabsorption (PA3 appears at τ = 0 fs in figure 4.8 (b)). To analyse the relaxation dynamics of the PA3 channel, the line profile at $h\nu$ = 1.65 eV is shown (figure 4.8 (d)). From the fitting with exponential curves, the PA3 decay results very fast and after a pump probe delay of about τ = 400 fs; a negative transient reflectivity signal with a long decay time is observed. In the 3D spectrum, a dark-purple zone corresponding to a negative transient reflectivity signal is evident around the point $h\nu$=1.95 eV, τ = 400 fs (figure 4.8 (e)). This negative zone extends up to 2 eV and appears after τ = 400 fs. In the reflectivity spectrum of figure 4.5 (b), the feature at about 2 eV has been ascribed to the TC transition in the metallic tubes. As the pump photon energy at 1.55 eV is unable to excite any transition in the metallic tube, the presence of this photo-bleaching channel, which implies a filling of

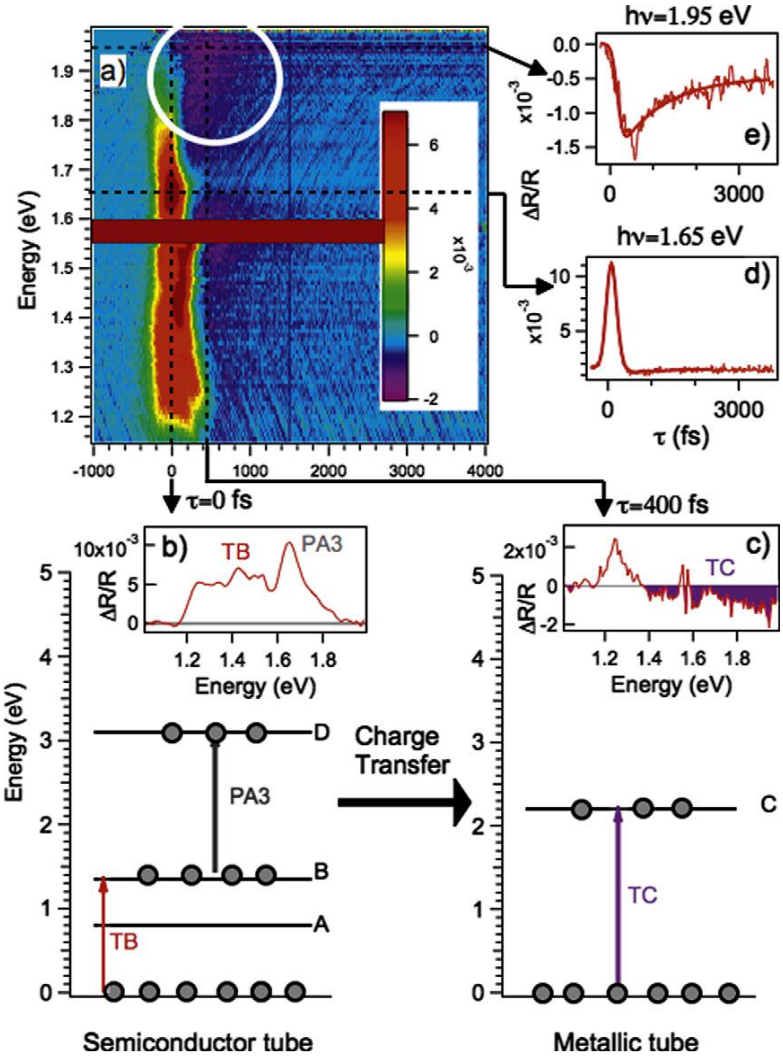

Figure 4.8: (a) 3D image of the time resolved reflectivity spectrum collected on unaligned SWCNT bundles by using the super continuum probe and a $h\nu$ = 1.55 eV pump. At the bottom: schemes of the charge transfer. At τ = 0 the carriers are excited in the B band of the semiconducting *tubes by the laser pulse. Some of the carriers are excited by the same pulse into the D band (PA3 transition in (b)). After 400 fs (c), carriers in the excited-states of semiconducting tube move towards the metallic tube and a negative TR signal due to TC transition appears in the probe spectrum. On the right, image profiles extracted at photon energies of the probe corresponding to PA3 (d) and TC transitions (e).*

the C band, is the evidence of a charge transfer from the semiconducting to

the metallic tube.

These observations can be interpreted considering that the pump laser excites a population in the B band of the semi-conducting SWCNTs. Some of the delocalized carriers are excited by the same pump pulse into the D band. By calculating the area of the transient reflectivity spectrum at $\tau = 0$ fs (figure 4.8 (b)), the intensity of the PA3 photoabsorption process can be estimated resulting comparable with that of free carriers excited in the B band. Because of their mobility, the carriers transfer from the semiconducting to the metallic tube within 400 fs, giving rise to a photobleaching of the transient reflectivity when the probe photon energy is nearly resonant with the TC transition. The lack of the B and C band photobleaching in the reflectivity spectrum reported in literature [18] confirms that the two mechanisms are mutually exclusive and that only the free electron behaviour of the excited carriers permits to switch on the semiconducting-metallic charge transfer.

The slow relaxation dynamics of the C photo bleaching (about 2 ps, see image profile at $h\nu$= 1.95 eV of figure 4.7 (e)) agrees with the dynamics of the photo bleaching channels reported in literature on SWCNTs. [20]

To perform a quantitative study of the transient reflectivity spectrum at $\tau = 0$ fs, a differential dielectric function model was fitted to the time-resolved-reflectivity data, $\Delta R/R=(R_{ex}(\varepsilon_{ex})-R_{eq}(\varepsilon_{eq}))/R_{eq}$, where R_{ex}, ε_{ex}, R_{eq}, ε_{eq} are the excited and equilibrium reflectivity and dielectric function, respectively. The ε_{eq} has been calculated by fitting R_{eq} (figure 4.5 (b)) with a sum of Lorentz oscillators, which represent the transitions TA, TB, TC, and TD.

According to the differential dielectric function model [44], for reproducing the transient reflectivity spectrum, it occurs to modify the fitting parameters of the Lorentz oscillators or to add new oscillators. In our case, to properly fit the differential spectrum $\Delta R/R$ (figure 4.8 (b)), we need to add one Drude and one Lorentz oscillator, the first to take into account the free electron mobility of the photoexcited carriers in the B band, and the

second to reproduce the PA3 photoabsorption at 1.7 eV. The presence of solitonic structures in the super continuum affects the fitting accuracy of the line profile at $\tau = 0$ fs with the differential model. However, it is possible to extrapolate a value for the plasma frequency in the Drude model (Eq. (1)) of $4x10^{15}$ sec^{-1} (2.5 eV) that corresponds to a carrier density of $4x10^{21}$ cm^{-3}. This value, compared with the carrier density excited by the laser pump $2x10^{20}$ cm^{-3} for a pump fluence of 0.2 mJ/cm^2 (Eq. 5.2)), confirms the delocalized character of the carriers excited in the B band of semiconducting tubes.

4.4 Conclusions

Time-resolved reflectivity measurements demonstrate that intertube interactions in bundled unaligned SWCNTs induce a free electron character to the photo excited carriers favouring a charge transfer from semiconducting to metallic tubes. This finding paves the way to new and important technologies closely connected to the intra- and inter-tube conductivity.

References

[1] P. Avouris, Z. Chen, and V. Perebeinos, Carbon-based Electronics, in Nanscience and Technology: A Collection of Reviews from Nature Journals, World Scientific 174-184, (2010).

[2] A. Jorio, G. Dresselhaus, and M. S. Dresselhaus, Carbon Naotubes: advanced topics in the synthesis, structure, properties and applications, Springer (2008).

[3] M. Bockrath, D. H. Cobden, P. L. McEuen, N. G. Chopra, A. Zettl, A. Thess, and R. E. Smalley, Science 275(5308), 1922-1925 (1997).

[4] V. Derycke, R. Martel, J. Appenzeller, and P. Avouris, Nano Lett. 1(9), 453-456 (2001).

[5] A. Rao, J. Chen, E. Richter, U. Schlecht, P. Eklund, R. Haddon, U. Venkateswaran, Y.-K. Kwon, and D. Tomanek, Phys. Rev. Lett. 86(17), 3895 (2001).

[6] S. Reich, J. Maultzsch, C. Thomsen, and P. Ordejon, Phys. Rev. B 66(3), 035412 (2002).
[7] F. Borondics, K. Kamarás, M. Nikolou, D. Tanner, Z. Chen, and A. Rinzler, Phys. Rev. B 74(4), 045431 (2006).
[8] U. Venkateswaran, A. Rao, E. Richter, M. Menon, A. Rinzler, R. Smalley, and P. Eklund, Phys. Rev. B 59(16), 10928 (1999).
[9] D. Kahn and J. P. Lu, Phys. Rev. B 60(9), 6535 (1999).
[10] L. Henrard, E. Hernandez, P. Bernier, and A. Rubio, Phys. Rev. B 60(12), R8521 (1999).
[11] J. Kürti, G. Kresse, and H. Kuzmany, Phys. Rev. B 58(14), R8869 (1998).
[12] P. Delaney, H. J. Choi, J. Ihm, S. G. Louie, and M. L. Cohen, Nature 391(6666), 466 (1998).
[13] Y.-K. Kwon, S. Saito, and D. Tománek, Phys. Rev. B 58(20), R13314 (1998).
[14] L. Alvarez, A. Righi, T. Guillard, S. Rols, E. Anglaret, D. Laplaze, and J.-L. Sauvajol, Chem. Phys. Lett. 316(3-4), 186-190 (2000).
[15] S. Reich, M. Dworzak, A. Hoffmann, C. Thomsen, and M. Strano, Phys. Rev. B 71(3), 033402 (2005).
[16] X. Blase, L. X. Benedict, E. L. Shirley, and S. G. Louie, Phys. Rev. Lett. 72(12), 1878 (1994).
[17] T. Hertel, R. Fasel, and G. Moos, Appl. Phys. A 75(4), 449-465 (2002).
[18] O. Korovyanko, C.-X. Sheng, Z. Vardeny, A. Dalton, and R. Baughman, Phys. Rev. Lett. 92(1), 017403 (2004).
[19] J.-S. Lauret, C. Voisin, G. Cassabois, C. Delalande, P. Roussignol, O. Jost, and L. Capes, Phys. Rev. Lett. 90(5), 057404 (2003).
[20] C. Manzoni, A. Gambetta, E. Menna, M. Meneghetti, G. Lanzani, and G. Cerullo, Phys. Rev. Lett. 94(20), 207401 (2005).
[21] L. Lüer, J. Crochet, T. Hertel, G. Cerullo, and G. Lanzani, ACS Nano 4(7), 4265-4273 (2010).
[22] M. Zheng and E. D. Semke, J. Am. Chem. Soc. 129(19), 6084-6085 (2007).

[23] S. Hofmann, R. Sharma, C. Ducati, G. Du, C. Mattevi, C. Cepek, M. Cantoro, S. Pisana, A. Parvez, and F. Cervantes-Sodi, Nano Lett. 7(3), 602-608 (2007).
[24] F. Cilento, C. Giannetti, G. Ferrini, S. Dal Conte, T. Sala, G. Coslovich, M. Rini, A. Cavalleri, and F. Parmigiani, Appl. Phys. Lett. 96(2), 021102 (2010).
[25] D. Davazoglou and V. E. Vamvakas, J. Electrochem. Soc. 150(5), F90-F96 (2003).
[26] M. K. Olsson, K. Macák, and W. Graf, Surf. & Coat. Technol. 1(124), 85 (2000).
[27] M. Ritala, M. Leskelä, J. P. Dekker, C. Mutsaers, P. J. Soininen, and J. Skarp, Chem. Vap. Deposition 5(1), 7-9 (1999).
[28] T. De Los Arcos, F. Vonau, M. Garnier, V. Thommen, H.-G. Boyen, P. Oelhafen, M. Düggelin, D. Mathis, and R. Guggenheim, Appl. Phys. Lett. 80(13), 2383-2385 (2002).
[29] L. Delzeit, B. Chen, A. Cassell, R. Stevens, C. Nguyen, and M. Meyyappan, Chem. Phys. Lett. 348(5-6), 368-374 (2001).
[30] L. Delzeit, I. McAninch, B. A. Cruden, D. Hash, B. Chen, J. Han, and M. Meyyappan, J. Appl. Phys. 91(9), 6027-6033 (2002).
[31] M. S. Dresselhaus, G. Dresselhaus, R. Saito, and A. Jorio, Phys. Rep. 409(2), 47-99 (2005).
[32] H. Kataura, Y. Kumazawa, Y. Maniwa, I. Umezu, S. Suzuki, Y. Ohtsuka, and Y. Achiba, Synth. Met. 103(1-3), 2555-2558 (1999).
[33] Y.-Z. Ma, L. Valkunas, S. L. Dexheimer, S. M. Bachilo, and G. R. Fleming, Phys. Rev. Lett. 94(15), 157402 (2005).
[34] K. Kato, K. Ishioka, M. Kitajima, J. Tang, R. Saito, and H. Petek, Nano Lett. 8(10), 3102-3108 (2008).
[35] Y. Murakami, E. Einarsson, T. Edamura, and S. Maruyama, Phys. Rev. Lett. 94(8), 087402 (2005).
[36] Y. Hashimoto, Y. Murakami, S. Maruyama, and J. Kono, Phys. Rev. B 75(24), 245408 (2007).
[37] S. Reich, C. Thomsen, and J. Maultzsch, Carbon Nanotubes: basic concepts and physical properties, John Wiley & Sons (2008).

[38] L. Perfetti, T. Kampfrath, F. Schapper, A. Hagen, T. Hertel, C. Aguirre, P. Desjardins, R. Martel, C. Frischkorn, and M. Wolf, Phys. Rev. Lett. 96(2), 027401 (2006).
[39] F. Wooten, Optical properties of solids, Academic Press (2013).
[40] K. Seibert, G. Cho, W. Kütt, H. Kurz, D. Reitze, J. Dadap, H. Ahn, M. Downer, and A. Malvezzi, Phys. Rev. B 42(5), 2842 (1990).
[41] G. Ostojic, S. Zaric, J. Kono, M. Strano, V. Moore, R. Hauge, and R. Smalley, Phys. Rev. Lett. 92(11), 117402 (2004).
[42] T. Hertel and G. Moos, Phys. Rev. Lett. 84(21), 5002 (2000).
[43] A. Hagen, G. Moos, V. Talalaev, and T. Hertel, Appl. Phys. A 78(8), 1137-1145 (2004).
[44] D. N. Basov, R. D. Averitt, D. Van Der Marel, M. Dressel, and K. Haule, Rev. Mod. Phys. 83(2), 471 (2011).